Electrochimica Acta 311 (2019) 150–159

Contents lists available at ScienceDirect

Electrochimica Acta

journal homepage: www.elsevier.com/locate/electacta

High performance silicon nanowires/ruthenium nanoparticles micro-supercapacitors

Yasmina Bencheikh [a, b, f], Maxime Harnois [c], Roxana Jijie [a], Ahmed Addad [d], Pascal Roussel [e], Sabine Szunerits [a], Toufik Hadjersi [b], Seddik El Hak Abaidia [f], Rabah Boukherroub [a, *]

[a] Univ. Lille, CNRS, Centrale Lille, ISEN, Univ. Valenciennes, UMR 8520 - IEMN, F-59000, Lille, France
[b] Research Center of Semiconductor Technology for Energy-2, Bd Frantz Fanon, BP 140, Alger 7 Merveilles, 16038, Algers, Algeria
[c] Département Microélectronique & Microcapteurs, UMR 6164, Université de Rennes 1 – Campus de Beaulieu, 263 Avenue du Général Leclerc – CS 74205, 35042, Rennes Cedex, France
[d] Univ. Lille, CNRS, UMR 8207 – UMET, F-59000, Lille, France
[e] Univ. Lille, CNRS, Centrale Lille, ENSCL, Univ. Artois, UMR 8181 - UCCS - Unité de Catalyse et Chimie du Solide, Lille, France
[f] Process materials and environment research unit (URMPE), Faculty of science of the engineer, University M'Hamed Bougara of Boumerdès (UMBB), 35000 Boumerdès, Algeria

ARTICLE INFO

Article history:
Received 7 November 2018
Received in revised form
13 April 2019
Accepted 14 April 2019
Available online 22 April 2019

Keywords:
Micro-supercapacitors
Silicon nanowires
Ruthenium nanoparticles
Solid-state devices

ABSTRACT

The continuous increase of small electronic devices calls for small energy storage components, commonly known as micro-supercapacitors, that can ensure autonomous operation of these devices. In this work, we propose a simple and straightforward method to achieve high energy and power densities of a silicon-based micro-supercapacitor, consisting of silicon nanowires decorated with ruthenium nanoparticles (Ru/Si NWs). The Si NWs are obtained through the common vapor-liquid-solid (VLS) growth mechanism, while a simple electroless process is used to deposit Ru nanoparticles. While silicon nanostructuration allows to increase the surface area, coating with Ru NPs introduces a pseudocapacitance necessary to attain high energy and power densities. The Ru/Si NWs micro-supercapacitor exhibits a specific capacitance of 36.25 mF cm^{-2} at a current density of 1 mA cm^{-2} in a neutral Na_2SO_4 electrolyte and a high stability over 25 000 cycles under galvanostatic charge-discharge at 1 mA cm^{-2}. A solid state supercapacitor is then fabricated with symmetric electrodes separated by a polyvinyl alcohol/sulfuric acid electrolyte. The device displays a specific capacitance of ~18 mF cm^{-2} at a current density of 1 mA cm^{-2} and a specific power density 0.5 mW cm^{-2}. This solid-state nanowire device also exhibits a good stability over 10 000 galvanostatic charge-discharge cycles.

1. Introduction

Supercapacitors, also known as ultracapacitors or electrochemical capacitors, have attracted great attention for energy storage owing to their high power density, superior rate capability, rapid charging/discharging rate, long cycle life, and safe operation [1]. Supercapacitors, depending on the charge storage mechanism, can be classified in two types: Electric double layer capacitors (EDLCs) and pseudocapacitors (or redox supercapacitors). While EDLCs store electric charges at the electrode surface-electrolyte interface, in pseudocapacitors, the capacitance arises from rapid redox reaction at the electrode surface [1].

Recent technological progress towards small scale and portable electronic devices calls for the development of miniaturized energy storage sources able to provide these devices with necessary energy to operate autonomously [2,3]. It is thus desirable to design micro-supercapacitors that can be easily integrated with electronics on the same chip.

Silicon is the basic semiconductor in microelectronics and thus represents an essential electrode material for the fabrication of micro-supercapacitors. The last decades have witnessed a huge body of work devoted to improve the performance of EDLCs using silicon based materials. One important aspect of this work was through the formation of silicon nanostructures to increase the

* Corresponding author.
E-mail address: rabah.boukherroub@univ-lille.fr (R. Boukherroub).

https://doi.org/10.1016/j.electacta.2019.04.083
0013-4686/

surface area. Initial studies in this area focused on the preparation of silicon nanowires (Si NWs) using the vapor-liquid-solid (VLS) growth mechanism of different morphologies and doping type and level [4–10]. To minimize surface oxidation and achieve stable performance, organic solvents or ionic liquids were used to operate the developed Si NWs-based micro-supercapacitors.

Following this work, another strategy was proposed to ensure stable performance of Si NWs micro-supercapacitors, prepared using VLS or metal-assisted chemical etching (MACE), in aqueous media through coating with silicon carbide [11], diamond [12,13], organic thin films [14–17], alumina layer [18], TiO_2 [19], and graphene [20]. Even though Si NWs coating enhanced significantly the stability of the electrode material, it was not possible to enhance the intrinsic capacitance of the electrode using this approach.

With the aim to improve the energy and power densities, recent studies focused on the use of hybrid materials through the introduction of NiO [21], MnO_x [22] MnO_2 [23], VO_x [24], and PEDOT [25]. Particularly, transition metal oxides, known as pseudocapacitive materials, are very promising for capacitance increase. The charge storage in these pseudocapacitive materials stems from their redox reactions, allowing rapid and reversible Faradaic surface reactions along with high charge-discharge rate.

Ru-based electrode materials represent an interesting category for designing supercapacitive electrodes owing to their excellent electrochemical properties, including high surface capacitance, rapid reversible redox process, and good cycling stability [26]. Silicon nanowires decorated with ruthenium nanoparticles (Ru/Si NWs) substrates have been reported in a few reports. For example, O'Brien et al. [27] prepared Ru/Si NWs by sputtering Ru NPs onto black silicon, obtained using the metal-assisted chemical etching (MaCE) technique, and successfully applied it for gas-phase CO_2 photomethanation. Ru/Si NWs, obtained through electroless deposition of Ru NPs from $RuCl_3$ precursor on hydrogenated Si NWs, were recently used for electrochemical hydrogen evolution reaction (HER) [28].

To the best of our knowledge, there is only one report on the preparation of ruthenium oxide/Si NWs electrode material for solid-state on chip supercapacitors [29]. In this work, the Si NWs were obtained through metal-assisted anodic etching, while a thin layer of ruthenium oxide was deposited using atomic layer deposition (ALD) at 290 °C. A specific capacitance of 19 mFcm^{-2} was recorded using cyclic voltammetry in Na_2SO_4 electrolyte at 5 mV s^{-1}. A solid state symmetric supercapacitor based on the modified electrode displayed a specific capacitance of 6.5 mF cm^{-2} at 2 mV s^{-1} with a good stability over 10 000 cycles [29].

In this study, we adopted the electroless deposition technique to decorate Si NWs, produced through the VLS growth mechanism, with Ru nanoparticles at room temperature. This approach is suitable to enhance energy storage capability by taking benefit of the high surface area of Si NWs and the pseudocapacitive properties of Ru nanoparticles. The resulting electrode exhibited a specific capacitance of 36.25 mF cm^{-2} and a retention higher than 87% upon 25 000 galvanostatic charge-discharge cycles at 1 mA/cm^2 in aqueous Na_2SO_4 electrolyte. The advantage of the fabricated electrode is its high performance and stability. Additionally, the room temperature process used in this work is compatible with the microelectronic fabrication processes (CMOS technology).

2. Experimental part

2.1. Materials and methods

All chemicals and reagents were of analytical grade and used without any purification. Ruthenium chloride hydrate ($RuCl_3 \times H_2O$), polyvinyl alcohol (PVA) powder, sodium sulfate (Na_2SO_4), hydrogen peroxide (H_2O_2, 30%), hydrofluoric acid (HF, 48%), nitric acid (HNO_3), and sulfuric acid (H_2SO_4) were obtained from Sigma-Aldrich (France).

The water used throughout the experiments was purified with a Milli-Q system from Millipore Co. (resistivity = 18 MΩ cm).

2.2. Preparation of silicon nanowires (Si NWs)

Single-side polished silicon (100) oriented n-type wafers (Siltronix, France) (arsenic-doped, 0.001–0.005 Ohm-cm^{-1} resistivity) were used as substrate. The substrate was degreased in acetone and isopropyl alcohol, rinsed with Milli-Q water, and cleaned in a piranha solution (3:1 concentrated H_2SO_4/30% H_2O_2) for 15 min at 80 °C followed by copious rinsing with Milli-Q water. The surface was further dried under a stream of nitrogen.

Silicon nanowires (Si NWs) used in this work were prepared using the vapor-liquid-solid (VLS) mechanism [30]. The fundamental process is based on metal-catalyst-directed chemical vapor deposition of silicon. First, a thin film of gold (4 nm thick) was evaporated on the clean Si substrate. Gold nanoparticles with a wide size distribution were obtained as a result of metal dewetting on the surface. Exposure of the gold-coated surface to silane gas at a pressure of 0.4 T (Q = 40 sccm) at 500 °C for 60 min led to Si NWs growth.

Safety Considerations: The mixture H_2SO_4/H_2O_2 (piranha) solution is a strong oxidant. It reacts violently with organic materials. It can cause severe skin burns. It must be handled with extreme care in a well-ventilated fume hood while wearing appropriate chemical safety protection. HF is a hazardous acid which can result in serious tissue damage if burns were not appropriately treated.

2.3. Preparation of silicon nanowires-ruthenium nanoparticles (Ru/Si NWs)

The ruthenium-coated Si NWs were obtained by a simple electroless method [31,32] using ruthenium salt. Briefly, the Si NWs substrate was immersed into an aqueous solution of $RuCl_3 \times H_2O$ (1 mM)/HF (0.15 M) for different times (30, 45, 60 and 75 min) at room temperature. The resulting interface was rinsed with water and dried under a gentle stream of nitrogen.

2.4. Solid state supercapacitor fabrication

To prepare the solid PVA/H_2SO_4 electrolyte, 0.5 g of PVA powder was slowly added into 5 mL of deionized water under magnetic stirring to completely dissolve the PVA. 281 µL of H_2SO_4 were added into the solution and heated in an oil bath at 85 °C until a homogeneous solution was obtained and then cooled down to room temperature.

The polymer-based electrolyte was drop casted on the nanowire electrodes (1 cm × 0.5 cm) and baked 10 min at 45 °C and kept in air to solidify the electrolyte.

2.5. Characterization

2.5.1. Scanning electron microscopy (SEM)

Scanning electron microscopy (SEM) images were obtained using an electron microscope ULTRA 55 (Zeiss) equipped with a thermal field emission emitter and three different detectors (EsB detector with filter grid, high-efficiency In-lens SE detector, Everhart-Thornley secondary electron detector).

2.5.2. X-ray diffraction (XRD)

X-ray diffraction (XRD) patterns were collected on a high flux Rigaku Smartlab rotated anode, working with a copper Kα radiation

(1.5418 ang) with an applied voltage of 45 kV and an anode current of 200 mA in the 2θ range of 25–90°. The beam was made parallel through a multilayer mirror and a reflection geometry was used. To avoid any saturation of the detector when it passes through the (004) peak of the substrate, the sample was 2° misoriented.

2.5.3. Transmission electron microscopy (TEM)

TEM analysis was performed on a TECNAT-G2 working at 200 kV, equipped with an EDS spectrometer. The Ru/SiNW composite was dispersed on a thin carbon film of a 3 mm diameter copper grid (See Fig. S1).

2.5.4. X-ray photoelectron spectroscopy (XPS)

X-ray photoelectron spectroscopy (XPS) measurements were performed with an ESCALAB 220 XL spectrometer from Vacuum Generators featuring a monochromatic Al Kα X-ray source (1486.6 eV) and a spherical energy analyzer operated in the CAE (constant analyzer energy) mode (CAE = 100 eV for survey spectra and CAE = 40 eV for high-resolution spectra), using the electromagnetic lens mode. No flood gun source was needed due to the conducting character of the substrates. The angle between the incident X-rays and the analyzer is 58°. The detection angle of the photoelectrons is 30°.

2.6. Electrochemical studies

Electrochemical studies were carried out using a potentiostat (Autolab, model 2.01, Methrom, France). Cyclic Voltammetry (CV), and galvanostatic charge-discharge measurements were conducted from −0.6 V to +0.2 V. Electrochemical Impedance Spectroscopy (EIS) was performed across the frequency range 1 MHz and 0.03 Hz with AC amplitude of 10 mV. All electrochemical tests were performed in 1 M Na_2SO_4 electrolyte aqueous solution using a typical three-electrode electrochemical cell configuration. Ruthenium-coated SiNWs substrate was used as the working electrode, Pt foil served as the counter electrode, and Ag/AgCl as the reference electrode. All the calculated values were normalized to the surface of the active electrode material (0.29 cm^2).

3. Results and discussion

The silicon nanowires (Si NWs) investigated in this study were produced by the well-known vapor-liquid-solid (VLS) growth mechanism [30]. In this growth process, Au nanoparticles, obtained through thin Au film (4 nm) dewetting on SiO_2/Si surface, act as catalytic sites for Si NWs growth. Under controlled conditions, the size of the Si NWs is determined by the size of the Au NPs and the length is defined by the growth time.

Scanning electron microscopy (SEM) images, depicted in Fig. 1, revealed a high density of nanowires with an average diameter in the range of 30–80 nm. The large distribution of the nanowires diameter is due to the size variation of the gold nanoparticles serving as catalysts for Si NWs growth.

Ruthenium nanoparticles (Ru NPs) were deposited on Si NWs through a simple electroless process at room temperature. The Si NWs substrates were first treated with 10% HF aqueous solution to remove the native silicon oxide layer and generate a hydrogen termination. Subsequent immersion in $RuCl_3$ aqueous solution for various times (30, 45, 60, 75 min) allowed Ru NPs loading on the Si NWs. Electroless deposition of metal nanoparticles on Si NWs and porous silicon substrates has been studied in many reports in the literature [28,33–35]. In the electroless mechanism, metal ions with redox potential greater than hydrogen are reduced by electrons from the Si atoms to metal atoms, Eq. (1).

$$Ru^{3+} + 3\ e^{-} \rightarrow Ru(s) \quad (1)$$

The deposited metal atoms first form nuclei, then nanoclusters and finally nanoparticles. During Ru deposition, the silicon surface is oxidized according to Eq. (2):

$$Si + 2H_2O \rightarrow SiO_2 + 4H^{+} + 4e2) \quad ^{-})$$

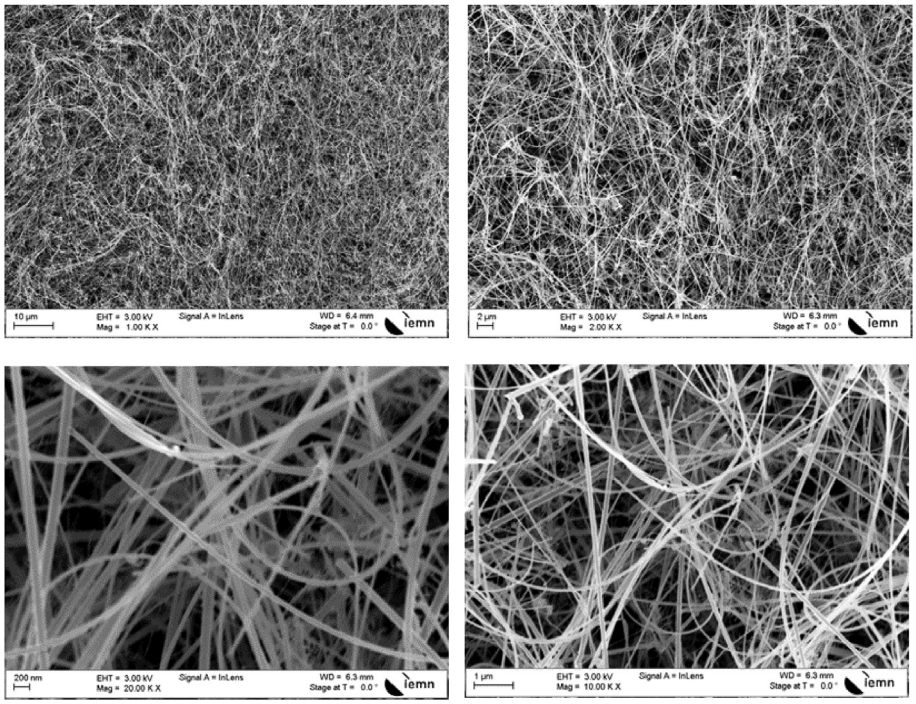

Fig. 1. SEM images of the Si NWs at different magnifications.

The role of HF is to dissolve the oxide layer and generate a fresh hydrogenated Si surface. Indeed, when the electroless process was performed in absence of HF, no particle deposition occurred after 30 min immersion, as evidenced from SEM imaging (data not shown). This is mainly due to electron transfer hindrance by the silicon dioxide barrier on the Si NWs surface.

To assess the influence of deposition time on the specific capacitance, the electroless deposition was performed in $RuCl_3$ (1 mM)/HF (0.15 M) aqueous solution at room temperature for various times (30, 45, 60 and 75 min). SEM imaging showed a continuous increase of the nanoparticles density on the Si NWs substrate upon increasing deposition time (Fig. 2). Up to 60 min, it is obvious that some of the nanowires are not coated with Ru NPs. A full coverage of the nanowires was attained after 75 min. This sample gave also the best specific capacitance (as discussed later), so additional characterizations were carried out on this sample. Also, the color of the samples turned from light gold (30 min) to dark (75 min), indicating a change of the optical properties of the samples (Insets in Fig. 2).

The XRD pattern of the initial Si NWs substrate comprises diffraction peaks at 2θ of 28.44°, 47.22° and 56.11° due to (111), (220) and (311) silicon planes, respectively (Fig. 3). The peaks at 38.22° and 44.44° are ascribed to Au terminating the nanowires, according to the VLS growth mechanism. The results are in accordance with data reported in the literature [36,37]. After, loading Ru NPs on the Si NWs *via* electroless deposition, the XRD pattern

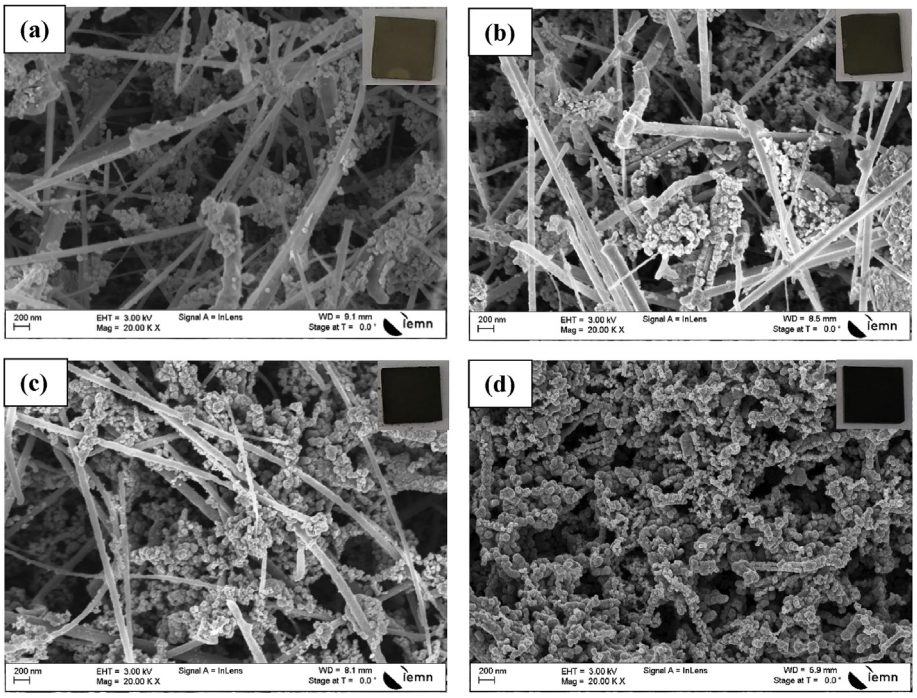

Fig. 2. SEM images of Ru/Si NWs for different deposition times in $RuCl_3$ (1 mM)/HF (0.15 M) aqueous solution at room temperature: 30 min (a), 45 min (b), 60 min (c) and 75 min (d). The insets are the corresponding optical images.

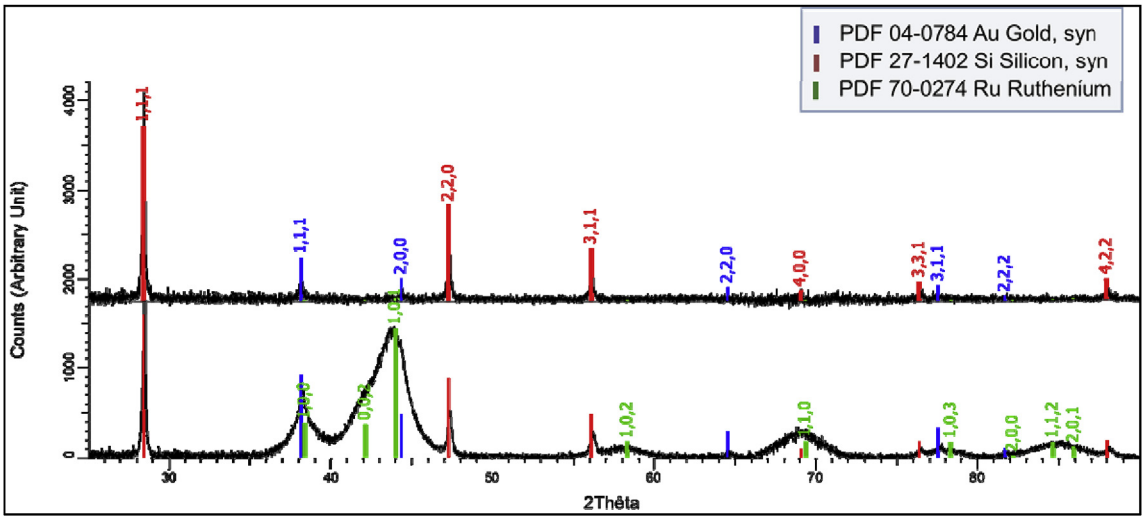

Fig. 3. X-ray diffraction (XRD) patterns of Si NWs (a) and Ru/Si NWs (b).

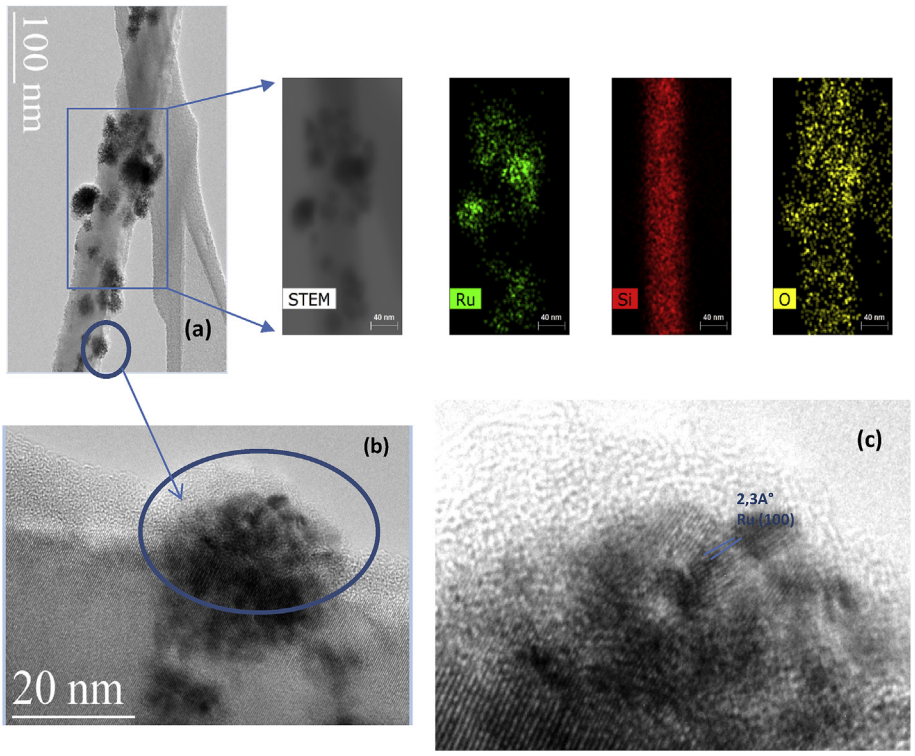

Fig. 4. (a) Scanning transmission electron microscopy (STEM) and elemental mapping, (b, c) TEM and high resolution TEM images of Ru NPs.

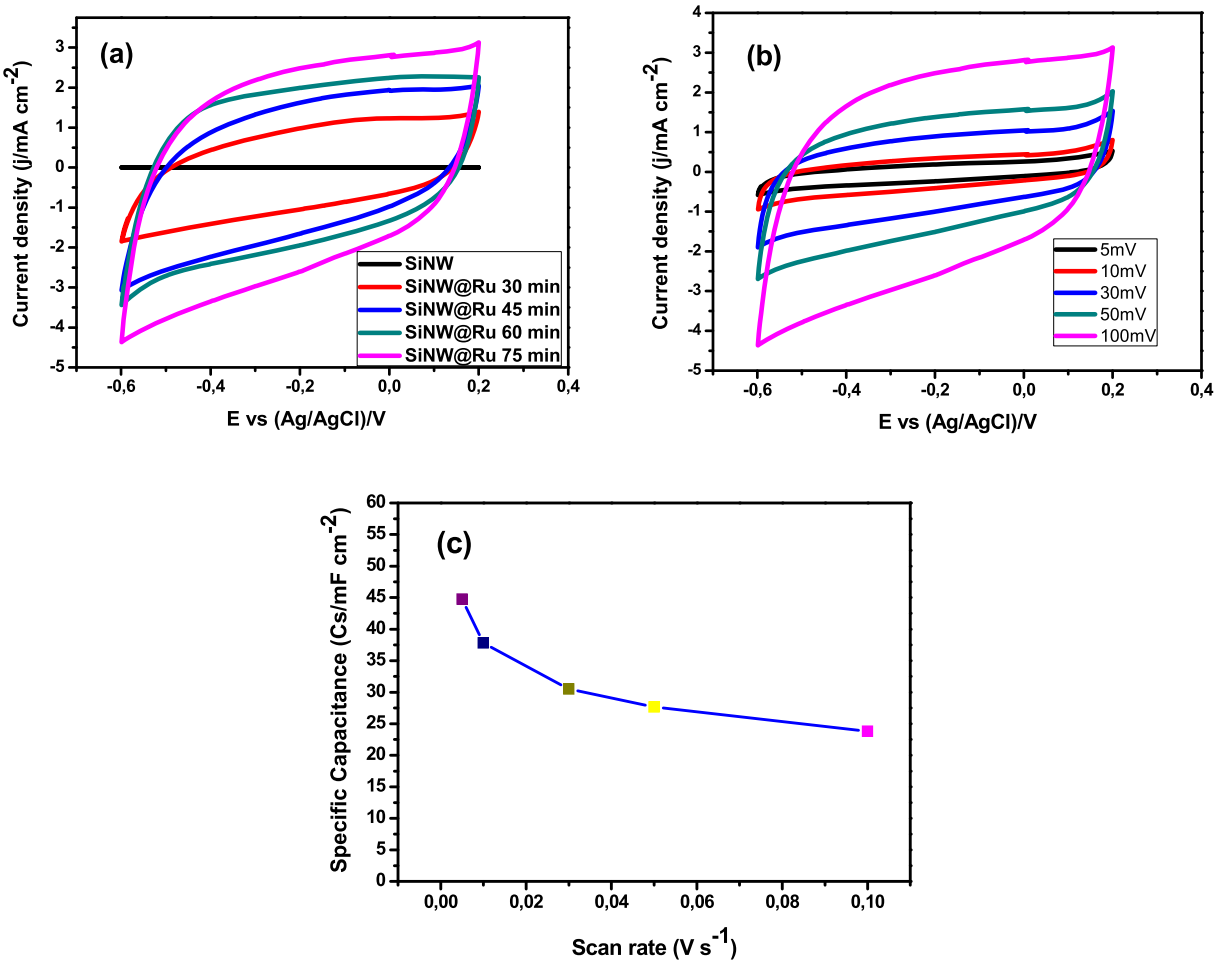

Fig. 5. (a) Cyclic voltammetry curves of Ru@SiNW electrode (75 min) recorded at a scan rate of 100 mA cm^{-2} in 1 M Na_2SO_4 aqueous solution for different deposition times, (b) C(V) responses at different scan rates (5–100 mV s^{-1}), (c) Effect of scan rate on specific capacitance.

exhibited additional broad XRD diffraction peaks at 2θ of 38.4° and 43.88° and other minor peaks, characteristic of Ru, along with the diffraction peaks due to Si and Au. All reflection peaks of the Ru/Si NWs can be easily indexed as pure structure of Ru^0, which is in good agreement with the literature data (JCPDS card 70-0274). Though the diffraction peaks of (100) and (101) are overlapped with (002) diffraction due to widening, the product should be the hexagonal phase [38]. According to Scherrer's equation ($d = k\lambda/\beta \cos\theta$), the mean size of particles is about 3–5 nm.

The Ru/Si NWs substrate was further characterized by transmission electron microscopy (TEM). Fig. 4a depicts a scanning transmission electron microscopy (STEM), in bright field, of a single Si NW decorated with Ru NPs. The diameter of a single Si NW is about 50 nm and the Ru NPs exhibit a small diameter between 3 and 6 nm, in accordance with XRD analysis. STEM characterization allows chemical contrast investigation. Elemental mapping of the Ru/Si NW clearly shows the presence of Si, Ru and O, in accordance with the chemical composition of the material. The presence of oxygen is most likely due to partial oxidation of silicon during exposure to ambient. Indeed, elemental mapping of a single Ru nanoparticle reveals a very small amount of oxygen, ruling out surface oxidation of the Ru NPs (Fig. S2).

Fig. 4b displays the TEM image of the Ru NPs on the silicon surface consisting of small nanocrystallites. The high resolution TEM image in Fig. 4c exhibits clear fringes for Ru NPs with a lattice spacing of 2.3 Å corresponding to the (100) interplanar distance of hexagonal Ru, in accordance with the XRD analysis.

X-ray photoelectron spectroscopy (XPS) was carried out to examine the chemical composition of the Si NWs substrate before and after loading Ru NPs. Figure S3 depicts the XPS survey spectrum of Ru/Si NWs. It comprises peaks due to Ru, Si, C and O elements. While Ru and Si are expected to originate from Ru/Si NWs, oxygen may be due to partial oxidation of the silicon core during sample handling and exposure to ambient. Part of the oxygen signal may also arise from surface contamination, as commonly encountered in XPS analysis. The presence of carbon is most likely due to

Table 1
Specific capacitance of Ru/Si NW electrode for different deposition times obtained from CV curves at 1 mA cm^{-2} in 1 M Na_2SO_4.

Deposition time (t/min)	30	45	60	75
IR (V)	0.1	0.05	0.03	0.03
Specific capacitance (C/mF cm^{-2})	12.5	22.66	23.37	36.25

Table 2
Specific capacitance values of Ru/Si NW (75 min) electrode obtained from CV curves at different scan rates 1 M Na_2SO_4.

Scan rate (Sr/mV s^{-1})	5	10	30	50	100
Specific capacitance (C/mF cm^{-2})	44.75	37.81	30.50	27.65	23.82

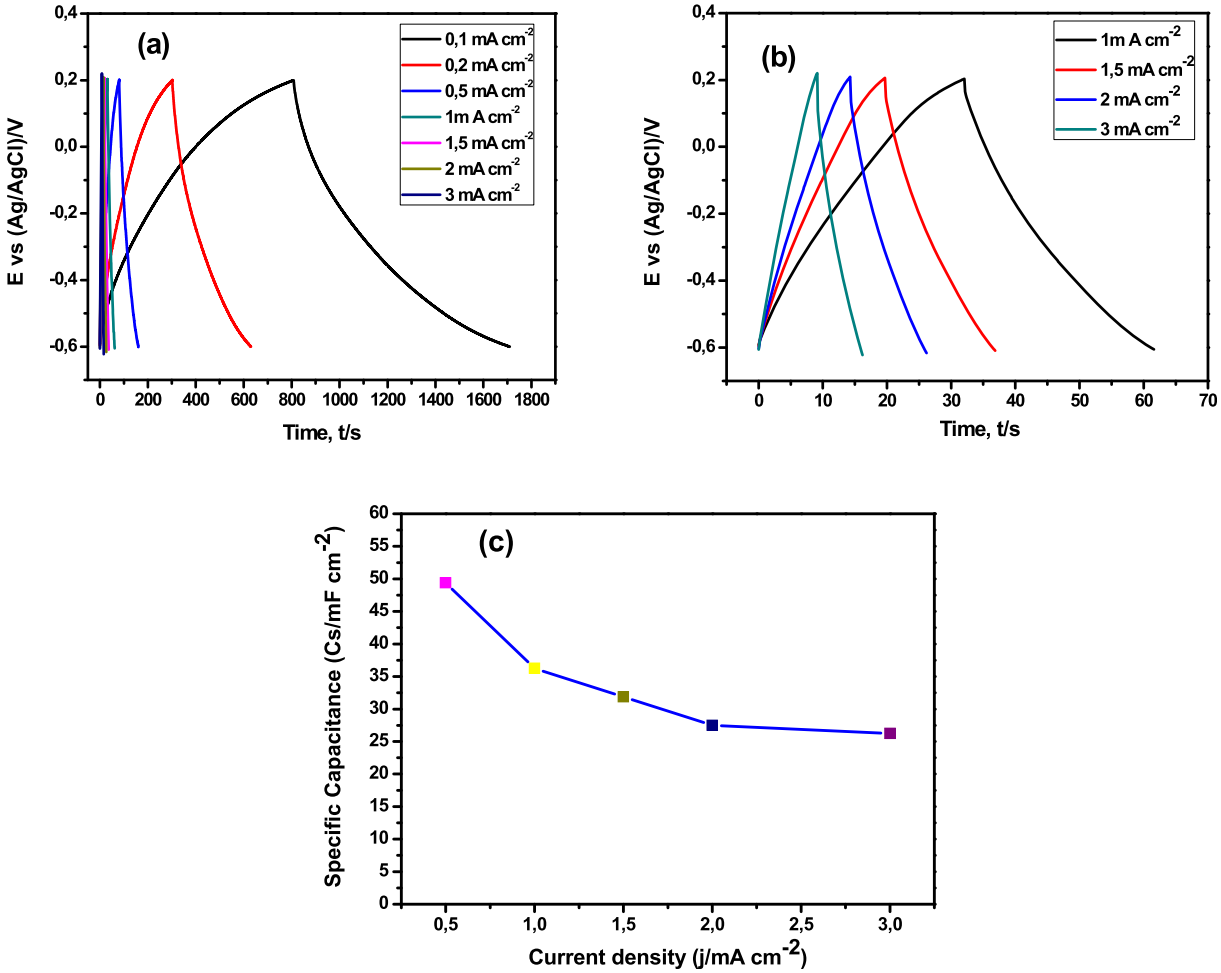

Fig. 6. Specific capacitance of Ru@SiNW electrode (75 min) obtained from galvanostatic charge-discharge curves recorded at different current densities in 1 M Na_2SO_4 aqueous solution.

surface contamination during sample handling and storage.

The high resolution XPS spectrum of the Ru_{3p} exhibits two symmetric doublets at 461.2 and 483.5 eV assigned to metallic $Ru_{3p3/2}$ and $Ru_{3p1/2}$, respectively with a spin orbit splitting of 22.3 eV characteristic of Ru in its metallic form [29,39], Fig. S4a. The absence of components at higher binding energies suggests that Ru is mainly in its metallic form, as expected for electroless deposition in $RuCl_3$/HF solution. The results are well in accordance with XRD and TEM measurements. The high resolution XPS spectrum of the O_{1s} can be deconvoluted into three peaks at 530.7, 531.7 and 533.5 eV ascribed to SiO_2, O_2^-/Si-O and OH/adsorbed water, respectively (Fig. S4b).

The electrical double layer capacitance of the resulting electrodes was analyzed utilizing cyclic voltammetry measurements in a 3 electrode configuration consisting of a platinum counter electrode, an Ag/AgCl wire reference electrode and Ru/Si NW working electrode. Electrical connection was made directly to the back side of the sample. Scans were recorded in the potential window of −0.6 to +0.2 V *vs.* Ag/AgCl electrode using 1 M Na_2SO_4 aqueous electrolyte. The specific capacitance was calculated from Equation (3):

$$C = \frac{\int jdV}{2 \times V \times r} \tag{3}$$

where j is the current density (A cm^{-2}), V is the potential window, r is the scan rate, and C is the specific capacitance; scan rates used for the measurements are 10, 20, 50 and 100 mV s^{-1}.

In addition, specific capacitance of the samples was calculated by using the following formula (4):

$$C = j\frac{dt}{dV} \tag{4}$$

The energy density (E) and power density (P) were determined by using equations (5) and (6), respectively:

$$E = \frac{1}{2}C(dV)^2 \tag{5}$$

and

$$P = \frac{E}{dt} \tag{6}$$

where dV is the potential range, j is the current density and dt is the total time of discharge.

Fig. 5a depicts the CV of Si NWs substrate recorded before and after decoration with Ru NPs for various deposition times (30, 45, 60 and 75 min) in 1 M Na_2SO_4 at a scan rate of 1 mA cm^{-2} in the potential window of −0.6 to + 0.2 V. The capacitance behavior of the Ru/Si NW electrodes is obvious from the rectangular shape of the CV curves with no apparent contribution from redox processes (Faradaic pseudocapacitance), suggesting that the specific capacitance is dominated by the electrochemical double layer capacitance. This result is in accordance with that recorded for Ru nanoparticles-reduced graphene oxide [40]. The specific capacitance values, deduced from the CV curves using Eq. (1), increased from 12.5 to 36.25 mF cm^{-2} upon increasing the deposition time from 30 to 75 min, respectively (Table 1). This can be explained by the increase of the Ru NPs density, as observed in SEM analysis.

Fig. 5b displays the CV curves of Ru/Si NWs (75 min) at different scan rates (5, 10, 30, 50, 100 mV s^{-1}) recorded in 1 M Na_2SO_4 aqueous solution at room temperature in the potential window of −0.6 to + 0.2 V. The results revealed that the electrodes maintained the rectangular shape, associated with adsorption-desorption of ions on the electrode surface, even at higher scan rates, indicating a good stability of the electrode material.

The specific capacitance values of Ru/Si NWs (75 min) at different scan rates, calculated from the CV plots, are exhibited in Fig. 5c and Table 2. It is evident that the specific capacitance decreases upon increasing the scan rate, because of insufficient ion

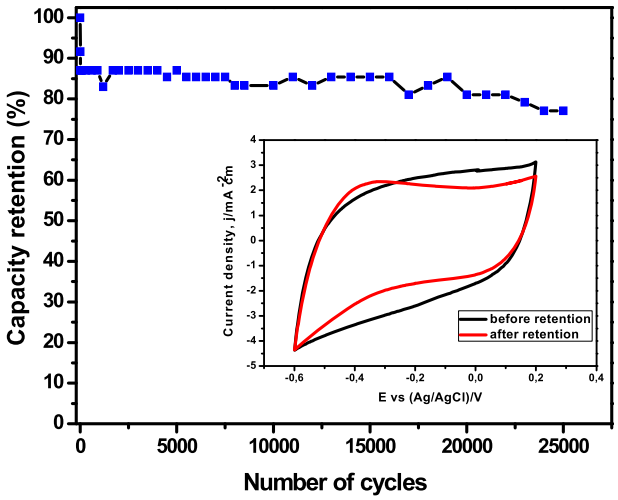

Fig. 7. Lifetime testing of the device performed using 25 000 complete charge–discharge cycles at a current density of 1 mA cm^{-2} between −0.6 and + 0.2 V. Inset shows the CV curves of the device before and after the cycling test at a scan rate of 100 V s^{-1}.

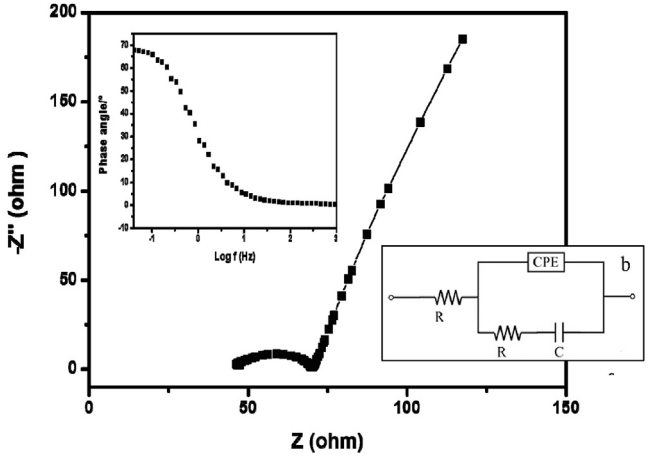

Fig. 8. Nyquist plot in the frequency range from 1 MHz to 0.1 Hz. Inset shows the Bode angle phase plot of the electrode.

Table 3
Galvanostatic charge-discharge plots at different applied current densities for Ru/Si NW in 1 M Na_2SO_4.

Current density (j/mA cm^{-2})	0.1	0.2	0.5	1	1.5	2	3
Specific capacitance (C/mF cm^{-2})	112.62	81.5	49.37	36.25	31.87	27.5	26.25
Specific power (mW cm^{-2})	0.0401	0.0807	0.199	0.386	0.377	0.802	1.292
Specific energy (E/mWH cm^{-2})	0.01	0.0072	0.0043	0.0032	0.0028	0.0024	0.0023

transport and adsorption.

Additionally, the specific capacitance of Ru/Si NWs (75 min) electrode was determined using the galvanostatic charge-discharge curves at different current densities in 1 M Na_2SO_4 (Fig. 6). The specific capacitance values are summarized in Table 3. Upon increasing the current density, the specific capacitance value decreases as follows: 112.62, 81.5, 49.37, 36.25, 31.87, 27.5 and 26.25 mF cm^{-2} at a current density of 0.1, 0.2, 0.5, 1, 1.5, 2 and 3 mA cm^{-2}, respectively.

The stability of an electrode material for supercapacitors is of prime importance to ensure its performance and long-term utilization. Fig. 7 depicts the stability test of the Ru/Si NWs electrode after 25 000 cycles. The electrode retains about 80% of its initial specific capacitance after 25 000 cycles at 1 mA cm^{-2} in the potential window between −0.6 and + 0.2 V in 1 M Na_2SO_4, indicating a good stability of the Ru/Si NWs electrode. The stability of Ru/Si NWs electrode after 25 000 cycles was additionally confirmed using CV (Inset Fig. 7) and SEM imaging (Fig. S5). Indeed, both the shape of the CV and the surface morphology were not altered significantly after the cycling experiment.

Electrochemical Impedance Spectroscopy (EIS) is a valuable tool to evaluate the electrode-electrolyte interface and understand the electronic transport of the Ru/Si NWs electrode. Fig. 8 exhibits the Nyquist plot within a frequency range from 1 MHz to 0.1 Hz at open circuit potential. The Nyquist plot was fitted using the Randles equivalent circuit (inset Fig. 8). In the high frequency region, a semi-circle was observed due to the charge transfer resistance (R_{CT}). In the low frequency region, a vertical plot was seen, suggesting a capacitive behavior of the electrode. The Bod plot in the inset, generated at lower frequency of 100 mHz, allows to determine a phase angle of 68°, which is lower than the value expected for an ideal capacitor (90°).

A symmetric solid state supercapacitor was fabricated from the Ru/Si NWs electrode according to the procedure described in the experimental section. Fig. 9a depicts the CV measurements carried out between −0.4 V and +0.4 V, a potential window where the device displayed rectangular CV curves, at various scan rates (5 mV s^{-1} to 50 mV s^{-1}). The results indicate good electrochemical performance and fast redox reaction of Ru/Si NWs electrode with PVA/H_2SO_4 gel electrolyte. The specific capacitance values extracted from the CV curves for each scan rate are plotted in Fig. 9b. A small decrease of the specific capacitance was observed upon increasing the scan rate up to 50 mV s^{-1} with a significant decrease at the higher scan rate tested (Table 4).

The solid-state symmetric supercapacitor was also tested in galvanostatic charge-discharge experiments at various current densities between 0 V and +0.8 V, as shown in Fig. 9c. The curves display a triangular shape with linear charge and discharge half

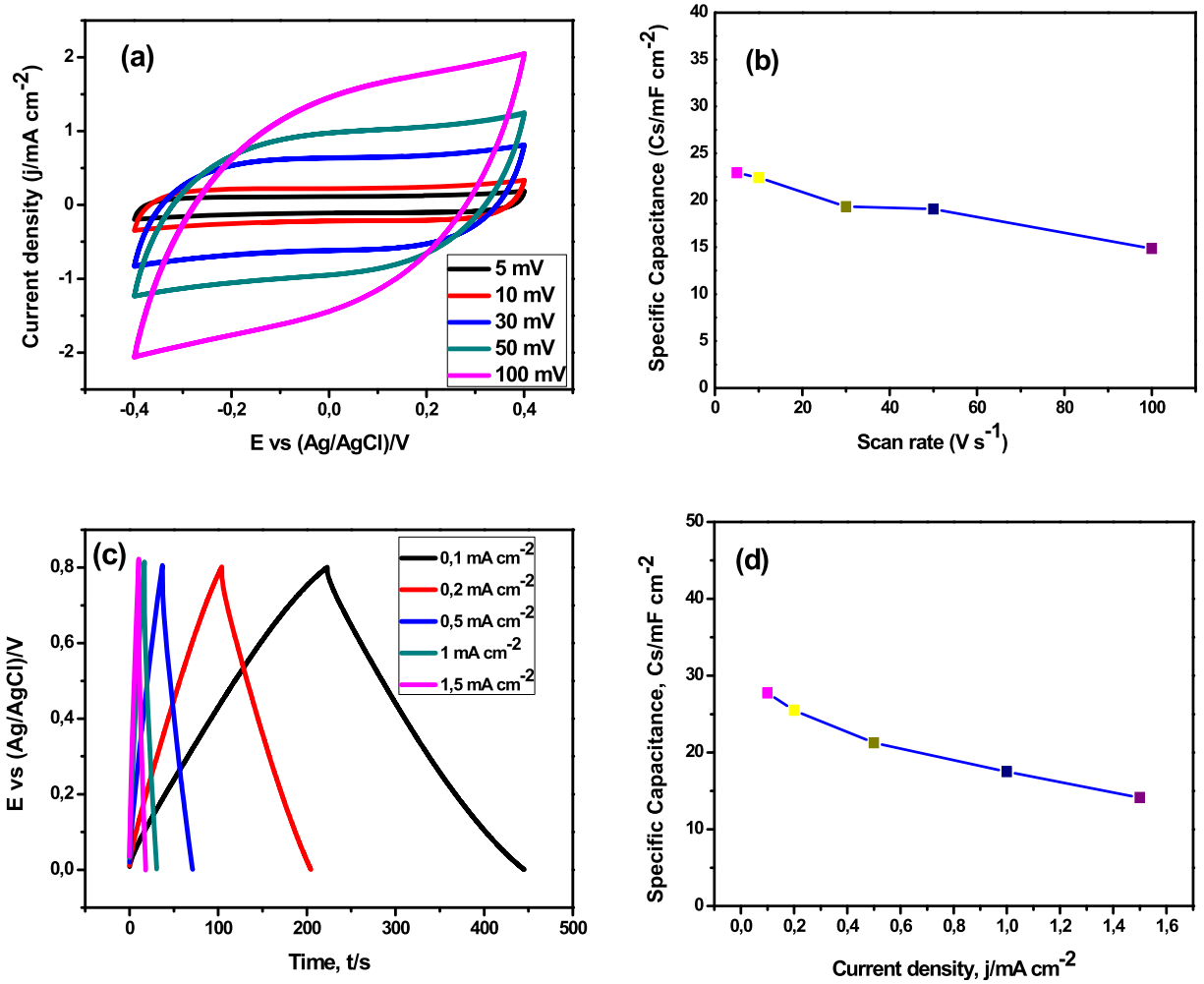

Fig. 9. (a) Cyclic voltammetry curves of symmetric solid state supercapacitor, consisting of Ru/Si NWs//PVA-H_2SO_4//Ru/Si NWs, recorded at a different scan rates, (b) Effect of scan rate on specific capacitance, (c) Galvanostatic charge-discharge curves at different current densities, (d) Effect of current density on specific capacitance.

Table 4
Specific capacitance values of the symmetric solid-state supercapacitor at different scan rates.

Scan rate (Sr/mV s^{-1})	5	10	30	50	100
Specific capacitance (C/mF cm^{-2})	22.94	22.41	19.34	19.06	14.84

Table 5
Specific capacitance values of the symmetric solid-state supercapacitor at different current densities.

Current density (j/mA cm^{-2})	0.1	0.2	0.5	1	1.5
Specific capacitance (C/mF cm^{-2})	27.75	25.5	21.25	17.5	14.125

cycles, typical of supercapacitors. The energy efficiency can be easily estimated from the capacity ratio between discharge and charge processes and is over 90.45% at 0.5 mA cm^{-2} current density. Similarly, the specific capacitance was calculated from the galvanostatic curves for different current densities (Fig. 9d). A similar trend was observed as previously with a continuous decrease of the specific capacitance with increasing the current density (Table 5).

The cycle stability of the device fabricated using Ru/Si NWs, obtained after 75 min of electroless deposition, was assessed by continuous charge-discharge measurements for a large number of cycles at a discharge current of 1 mA cm^{-2}. According to Fig. 10, the initial maximum specific capacity value of 17.5 mF cm^{-2} only decreased slightly to 16.88 mF cm^{-2} after 10 000 cycles. The 3.53% decrease relative to the initial capacitance reveals the reliable cyclability of our symmetric solid state capacitor; the repetitive charge-discharge cycles did not induce noticeable degradation of the hybrid Ruthenium-nanowire silicon array structure.

The high areal capacitance values determined for the Ru/Si NW symmetric supercapacitor are also superior to those found for most of other recently reported silicon nanowires-based symmetric micro-supercapacitors [41,42]: (1.9 mF cm^{-2} at 2 mA cm^{-2}) for MSC based on diamond-coated Si NW electrodes in ionic liquid Et_3NH-TFSI electrolyte [25], (14 mF cm^{-2} at 0.4 mA cm^{-2}) for MnO_2@-SiNWs hybrid symmetric micro-supercapacitors [23] and 2.3 mF cm^{-2} at 0.4 mA cm^{-2} for Si NW@RuO_x electrode based solid-state device with ALD deposition [29].

Fig. 11 depicts the Ragone plot i.e. power density (P/mW cm^{-2}) *vs*. energy density (E/mJ cm^{-2}) with comparison to other reported values. The electrode material exhibits power and energy densities

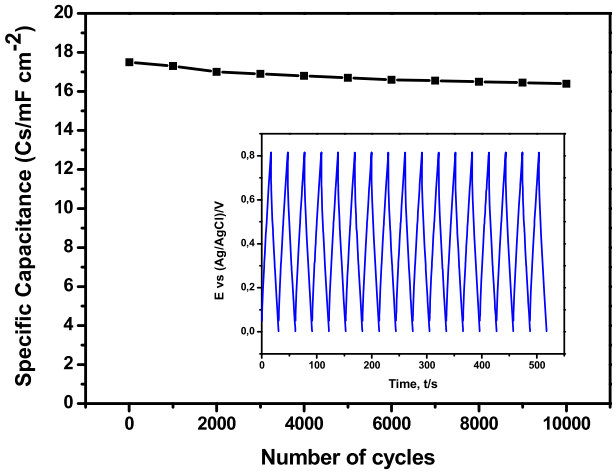

Fig. 10. Lifetime testing of the symmetric solid state supercapacitor device performed using 10 000 complete charge–discharge cycles at a current density of 1 mA cm^{-2} between 0 and + 0.8 V. The inset is the first corresponding charge-discharge curves.

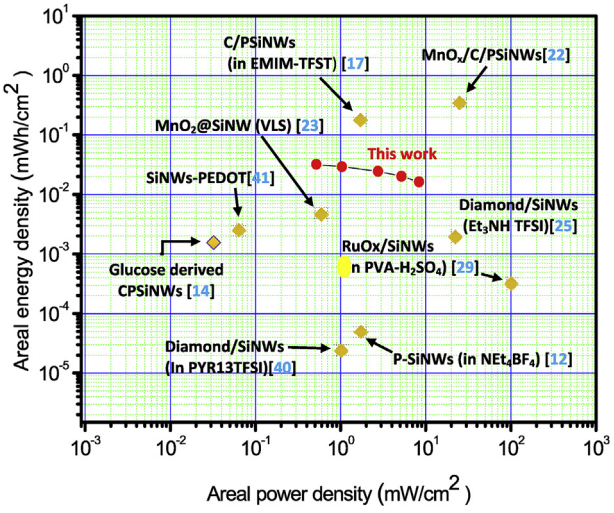

Fig. 11. Ragone plot of the symmetric solid state supercapacitor at different current densities and a comparison to other reported Si NWs-based supercapacitors.

ranging from 0.5 to 8.5 mWh cm^{-2} and from 1.5×10^{-2} to 3.5×10^{-2} mW cm^{-2}, respectively.

4. Conclusion

This paper describes a simple method for the fabrication of a symmetric solid-state micro-supercapacitor using silicon nanowire substrates decorated with ruthenium nanoparticles (Ru/Si NWs). The Ru nanoparticles are easily decorated on the Si NWs using electroless deposition technique in a hydrofluoric acid aqueous solution containing Ru ions at room temperature. We have investigated the effect of deposition time on the specific capacitance of the Ru/Si NWs electrode. Under optimized conditions, the Ru/Si NWs displayed a specific capacity as high as 112 mF cm^{-2} at an applied current density of 0.1 mA cm^{-2} in 1 M Na_2SO_4. The performance of a micro-supercapacitor, consisting of two identical Ru/Si NWs electrodes, was investigated electrochemically in 0.5 M H_2SO_4/PVA solid electrolyte. A specific capacitance of ~28 mF cm^{-2} and a specific power density of 0.5 mW cm^{-2} were obtained. This solid-state nanowire device also exhibited a good stability over 10 000 galvanostatic charge-discharge cycles. The technique reported in this work is simple and can be implemented for other metal ions to develop various micro-supercapacitors. Additionally, the process takes place at room temperature which is compatible with microelectronic processing technology.

Acknowledgement

Financial support from the Centre National de la Recherche Scientifique (CNRS), the University of Lille, and the Hauts-de-France region is gratefully acknowledged. The silicon nanowires have been fabricated using equipments of the NanoRennes platform.

Appendix A. Supplementary data

Supplementary data to this article can be found online at https://doi.org/10.1016/j.electacta.2019.04.083.

References

[1] M.S. Halper, J.C. Ellenbogen, Supercapacitors: A Brief Overview, Copyright © 2006, The MITRE Corporation, McLean, Virginia, USA, 2006.
[2] M. Beidaghi, Y. Gogotsi, Capacitive energy storage in micro-scale devices:

recent advances in design and fabrication of microsupercapacitors, Energy Environ. Sci. 7 (2014) 867–884.
[3] N.A. Kyerematenng, T. Brousse, D. Pech, Microsupercapacitors as miniaturized energy storage components for on-chip electronics, Nat. Nanotechnol. 12 (2017) 7–15.
[4] F. Thissandier, A. Le Comte, O. Crosnier, P. Gentile, G. Bidan, E. Hadji, T. Brousse, S. Sadki, Highly doped silicon nanowires based electrodes for micro-electrochemical capacitor applications, Electrochem. Commun. 25 (2012) 109–111.
[5] F. Thissandier, L. Dupré, P. Gentile, T. Brousse, G. Bidan, D. Buttard, S. Sadki, Ultra-dense and highly doped SiNWs for micro-supercapacitors electrodes, Electrochim. Acta 117 (2014) 159–163.
[6] F. Thissandier, P. Gentile, T. Brousse, G. Bidan, S. Sadki, Are tomorrow's micro-supercapacitors hidden in a forest of silicon nanotrees? J. Power Sources 269 (2014) 740–746.
[7] F. Thissandier, P. Gentile, N. Pauc, T. Brousse, G. Bidan, S. Sadki, Tuning silicon nanowires doping level and morphology for highly efficient micro-supercapacitors, Nano Energy 5 (2014) 20–27.
[8] D. Aradilla, P. Gentile, G. Bidan, V. Ruizd, P. Gómez-Romero, T.J.S. Schubert, H. Sahine, E. Frackowiak, S. Sadki, High performance of symmetric micro-supercapacitors based on silicon nanowires using N-methyl-N-propylpyrrolidinium bis(trifluoromethylsulfonyl)imide as electrolyte, Nano Energy 9 (2014) 273–281.
[9] F. Thissandier, N. Pauc, T. Brousse, P. Gentile, S. Sadki, Micro-ultracapacitors with highly doped silicon nanowires electrodes, Nanoscale Res. Lett. 8 (2013) 38.
[10] D. Gaboriau, D. Aradilla, M. Brachet, J. Le Bideau, T. Brousse, G. Bidan, P. Gentile, S. Sadki, Silicon nanowires and nanotrees: elaboration and optimization of new 3D architectures for high performance on-chip supercapacitors, RSC Adv. 6 (2016) 81017–81027.
[11] J.P. Alper, M. Vincent, C. Carraro, R. Maboudian, Silicon carbide coated silicon nanowires as robust electrode material for aqueous micro-supercapacitor, Appl. Phys. Lett. 100 (2012), 163901.
[12] D. Aradilla, F. Gao, G. Lewes-Malandrakis, W. Müller-Sebert, D. Gaboriau, P. Gentile, B. Iliev, T. Schubert, S. Sadki, G. Bidan, C.E. Nebel, A step forward into hierarchically nanostructured materials for high performance micro-supercapacitors: diamond-coated SiNW electrodes in protic ionic liquid electrolyte, Electrochem, Commun. Now. 63 (2016) 34–38.
[13] D. Aradilla, F. Gao, G. Lewes-Malandrakis, W. Müller-Sebert, P. Gentile, S. Pouget, C.E. Nebel, G. Bidan, Powering electrodes for high performance aqueous micro-supercapacitors: diamond-coated silicon nanowires operating at a wide cell voltage of 3 V, Electrochim. Acta 242 (2017) 173–179.
[14] R.R. Devarapalli, S. Szunerits, Y. Coffinier, M.V. Shelke, R. Boukherroub, Glucose-derived porous carbon-coated silicon nanowires as efficient electrodes for aqueous micro-supercapacitors, ACS Appl. Mater. Interfaces 8 (2016) 4298–4302.
[15] R. Kumar, A. Soam, R.O. Dusane, P. Bhargava, Sucrose derived carbon coated silicon nanowires for supercapacitor application, J. Mater. Sci. Mater. Electron. 29 (2018) 1947–1954.
[16] L. Sun, X. Wang, K. Zhang, J. Zou, Z. Yan, X. Hu, Q. Zhang, Bi-functional electrode for UV detector and supercapacitor, Nano Energy 15 (2015) 445–452.
[17] J.P. Alper, S. Wang, F. Rossi, G. Salviati, N. Yiu, C. Carraro, R. Maboudian, Selective ultrathin carbon sheath on porous silicon nanowires: materials for extremely high energy density planar micro-supercapacitors, Nano Lett. 14 (2014) 1843–1847.
[18] D. Gaboriau, M. Boniface, A. Valero, D. Aldakov, T. Brousse, P. Gentile, S. Sadki, Atomic layer deposition alumina-passivated silicon nanowires: probing the transition from electrochemical double-layer capacitor to electrolytic capacitor, ACS Appl. Mater. Interfaces 9 (2017) 13761–13769.
[19] F. Konstantinou, A. Shougee, T. Albrecht, K. Fobelets, TiO_2 coated Si nanowire electrodes for electrochemical double layer capacitors in room temperature ionic liquid, J. Phys. D Appl. Phys. 50 (2017), 415503.
[20] A. Soam, P. Kavle, A. Kumbhar, R.O. Dusane, Performance enhancement of micro-supercapacitor by coating of graphene on silicon nanowires at room temperature, Curr. Appl. Phys. 17 (2017) 314–320.
[21] F. Lu, M. Qiu, X. Qi, L. Yang, J. Yin, G. Hao, X. Feng, J. Li, J. Zhong, Electrochemical properties of high-power supercapacitors using ordered NiO coated Si nanowire array electrodes, Appl. Phys. A 104 (2011) 545–550.
[22] S. Ortaboy, J.P. Alper, F. Rossi, G. Bertoni, G. Salviati, C. Carraro, R. Maboudian, MnOx-decorated carbonized porous silicon nanowire electrodes for high performance supercapacitors, Energy Environ. Sci. 10 (2017) 1505–1516.
[23] D.P. Dubal, D. Aradilla, G. Bidan, P. Gentile, T.J.S. Schubert, J. Wimberg, S. Sadki, P. Gomez-Romero, 3D hierarchical assembly of ultrathin MnO_2 nanoflakes on silicon nanowires for high performance micro-supercapacitors in Li- doped ionic liquid, Sci. Rep. 5 (2015), 09771.
[24] Z. Li, F. Wang, X. Wang, Hierarchical branched vanadium oxide nanorod@Si nanowire architecture for high performance supercapacitors, Small 13 (2017) 1603076.
[25] D. Aradilla, F. Gao, G. Lewes-Malandrakis, W. Müller-Sebert, P. Gentile, M. Boniface, D. Aldakov, B. Iliev, T.J.S. Schubert, C.E. Nebel, G. Bidan, Designing 3D multihierarchical heteronanostructures for high-performance on-chip hybrid supercapacitors: poly(3,4-(ethylenedioxy)thiophene)-coated diamond/silicon nanowire electrodes in an aprotic ionic liquid, ACS Appl. Mater. Interfaces 8 (2016) 18069–18077.
[26] Q. Li, S. Zheng, Y. Xu, H. Xue, H. Pang, Ruthenium based materials as electrode materials for supercapacitors, Chem. Eng. J. 333 (2018) 505–518.
[27] P.G. O'Brien, A. Sandhel, T.E. Wood, A.A. Jelle, L.B. Hoch, D.D. Perovic, C.A. Mims, G.A. Ozin, Photomethanation of gaseous CO_2 over Ru/silicon nanowire catalysts with visible and near-infrared photons, Adv. Sci. 1 (2014), 1400001.
[28] L. Zhu, Q. Cai, F. Liao, M. Sheng, B. Wu, M. Shao, Ru-modified silicon nanowires as electrocatalysts for hydrogen evolution reaction, Electrochem. Commun. 52 (2015) 29–33.
[29] W. Zheng, Q. Cheng, D. Wang, C.V. Thompson, High-performance solid-state on-chip supercapacitors based on Si nanowires coated with ruthenium oxide via atomic layer deposition, J. Power Sources 341 (2017) 1–10.
[30] N. Verplanck, E. Galopin, J.-C. Camart, V. Thomy, Y. Coffinier, R. Boukherroub, Reversible electrowetting on superhydrophobic silicon nanowires, Nano Lett. 7 (2007) 813–817.
[31] N. Megouda, Y. Cofininier, S. Szunerits, T. Hadjersi, O. Elkechai, R. Boukherroub, Photocatalytic activity of silicon nanowires under UV and visible light irradiation, Chem. Commun. 47 (2011) 991–993.
[32] O. Fellahi, M.R. Das, Y. Coffinier, S. Szunerits, T. Hadjersi, M. Maamache, R. Boukherroub, Silicon nanowire arrays-induced graphene oxide reduction under UV irradiation, Nanoscale 3 (2011) 4662–4669.
[33] T. Tsuboi, T. Sakka, Y.H. Ogata, Metal deposition into a porous silicon layer by immersion plating: influence of halogen ions, J. Appl. Phys. 83 (1998) 4501–4506.
[34] O. Fellahi, A. Barras, G.-H. Pan, Y. Coffinier, T. Hadjersi, M. Maamache, S. Szunerits, R. Boukherroub, Reduction of Cr(VI) to Cr(III) using silicon nanowire arrays under visible light irradiation, J. Hazard Mater. 304 (2016) 441–447.
[35] N. Megouda, Y. Cofininier, S. Szunerits, T. Hadjersi, O. ElKechai, R. Boukherroub, Photocatalytic activity of silicon nanowires under UV and visible light irradiation, Chem. Commun. 47 (2011) 991–993.
[36] M. Lu, M.K. Li, L.B. Kong, X.Y. Guo, H.L. Li, Silicon quantum-wires arrays synthesized by chemical vapor deposition and its micro-structural properties, Chem. Phys. Lett. 374 (2003) 542–547.
[37] H. Jian, M. Dayan, X. Kewei, Growth and morphology modulation of needle-like silicon nanowires for SERS application, Rare Metal Mater. Eng. 44 (2015) 2692–2697.
[38] N.G. Garcia-Pena, R. Redon, A. Herrera-Gomez, A.L. Fernandez-Osorio, M. Bravo-Sanchez, G. Gomez-Sosa, Solventless synthesis of ruthenium nanoparticles, Appl. Surf. Sci. 340 (2015) 25–34.
[39] D.J. Morgan, Resolving ruthenium: XPS studies of common ruthenium materials, Surf. Interface Anal. 47 (2015) 1072–1079.
[40] H.K. Hassan, N.F. Atta, M.M. Hamed, A. Galal, T. Jacob, Ruthenium nanoparticles-modified reduced graphene prepared by a green method for high performance supercapacitor application in neutral electrolyte, RSC Adv. 7 (2017) 11286–11296.
[41] F. Gao, G. Lewes-Malandrakis, M.T. Wolfer, W. Müller-Sebert, P. Gentile, D. Aradilla, T. Schubert, C.E. Nebel, Diamond-coated silicon wires for supercapacitor applications in ionic liquids, Diamond Relat, Materials 51 (2015) 1–6.
[42] D. Aradilla, G. Bidan, P. Gentile, P. Weathers, F. Thissandier, V. Ruiz, P. Gomez Romero, T.J.S. Schubert, H. Sahin, S. Sadki, Novel hybrid micro-supercapacitor based on conducting polymer coated silicon nanowires for electrochemical energy storage, RSC Adv. 4 (2014) 26462–26467.